Selective production of ethylene via continuous oxidative dehydrogenation of ethane in (Dy_2O_3/MgO)-(Li-K)Cl composite membrane reactor

Maoshuai Li[a, b], André C. van Veen[b, *]

Andre.vanVeen@warwick.ac.uk

[a] Key Laboratory for Green Chemical Technology of Ministry of Education, Collaborative Innovation Center of Chemical Science and Engineering, School of Chemical Engineering & Technology, Tianjin University, Tianjin 300350, China

[b] School of Engineering, The University of Warwick, Coventry CV4 7AL, United Kingdom

[*] Corresponding author.

Tel: +44(0)2450933; email: Andre.vanVeen@warwick.ac.uk

Abstract:

Highly selective production of ethylene via continuous oxidative dehydrogenation of ethane has been established in the oxygen conductive (Dy_2O_3/MgO)-(Li-K)Cl composite membrane reactor. The disk-shape membrane was fabricated by pellet-pressing and characterised in terms of nitrogen physisorption, XRD and SEM. Specific surface area and pore volume decreases with increasing chlorides content with invariable values ≥10.6% chlorides content. SEM analysis reveals exposure of chlorides particles on the membrane surface. The presence of alkali chlorides promoted conversion of ethane selective to ethylene. The membrane reaction exhibited higher selectivity of ethylene than the fixed bed reaction. Reaction over 10.6% chlorides loaded membrane delivered highest ethylene selectivity (98%) and largest specific ethylene formation rate. Extended contact time and higher temperature served to further enhance ethylene yield.

Keywords: Ethane; Ethylene; Oxidative dehydrogenation; (Dy_2O_3/MgO)-(Li/K)Cl; Membrane reactor

1 Introduction

Ethylene is a critical commodity chemical, used as building block for the manufacture of plastics, detergents, surfactants and automotive antifreeze [1]. The worldwide production currently reaches over 150 million tonnes/year with an increasing demand forecast in the near future [2]. Industrial production of ethylene draws on (endothermic) steam cracking of ethane, naphtha and/or heavier hydrocarbons at temperature > 1050 K. High energy demand, low selectivity (70–80%) to ethylene and loss of valuable feedstock from coke formation are decided drawbacks that drive for the search of more efficient routes to ethylene [3]. Oxidative dehydrogenation of ethane represents an alternative to ethylene production. This reaction has been studied in a continuous flow fixed bed reactor using perovskite-type oxides (e.g., $La_{1-x}Sr_xFeO_{3-\delta}X_\delta$ [4], $YBa_2Cu_3O_{7-\delta}X_\delta$ [5], $La_{1.85}Sr_{0.15}CuO_{4-\delta}X_\delta$ [6] (X = F, Cl)) at high temperature (T = 873–973 K) and (e.g., Al_2O_3, TiO_2, ZrO_2, MgO and MCM-41) supported metal oxides (vanadium oxide [7–11], molybdenum oxide [12–15], nickel oxide [16–18] and chromium oxides [19]) at medium temperature (T = 673–873 K). Selective conversion of ethane to ethylene (up to 80% selectivity) was achieved over $YBa_2Cu_3O_{7-\delta}F_\delta$ [5] and V_2O_5/ZrO_2 [20]. Elevated selectivity (80–90%) has been reported for reaction over unsupported mixed metal oxides (MoVSb oxide [21] [21], MoVTeNb oxide [22–24], Ni-M−O (M = Ta [3], Nb [25], Ti [26], W [27], Sn [28])) at low temperature (T = 523–673 K). Supported alkali chloride catalysts have been demonstrated to deliver a high olefin selectivity in the oxidative dehydrogenation of ethane. Lercher et al. [29,30] has recorded up to 95% selectivity to ethylene over ($MgO\text{-}Dy_2O_3$) supported mixed molten alkali chlorides (LiCl-KCl) using a plug flow reactor (T = 898 K, $P(O_2)=P(C_2H_6)$=70mbar). But a discontinuous process suffers drawbacks in terms of production efficiency relative to continuous mode. In addition, use of pure oxygen or enriched oxygen increases process cost and coexistence of ethane and oxygen leads to undesired combustion reactions.

Oxygen-permeable membrane reactors serve to separate/transport oxygen which can circumvent use of pure oxygen as feedstock and direct contact of ethane with oxygen [31]. A search through literature found 80% selectivity to ethylene recorded for reaction (T = 1148 K) using $Bi_{1.5}Y_{0.3}Sm_{0.2}O_3$ ceramic tubular membrane reactor [32] and up to 90% selectivity (at 0.03–0.23 conversion) reported for reaction using $Ba_{0.5}Sr_{0.5}Co_{0.8}Fe_{0.2}O_{3-\delta}$ perovskite-type oxide membrane reactor (T = 923 K) [33]. It has been reported that chlorides doped ceria composite as electrolyte in fuel cell exhibit high oxygen ionic conductivity (≥698 K) where the molten chlorides and the chlorides-ceria interface can serve as conduction paths for oxygen ions [34]. Alkali chlorides (LiCl-KCl) on Dy_2O_3/MgO have been shown to activate/dissociate oxygen at the chlorides-solid interphase that can diffuse through the interface to the surface [35]. This implies this material is capable of transporting oxygen and could be used as oxygen-permeable membrane material. A search through the literature did not produce any reported application of Dy_2O_3/MgO-alkali chlorides composite membrane in the oxidative dehydrogenation of ethane for continuous production of ethylene. In this study, we examine oxygen permeability of (Dy_2O_3/MgO)-(Li-K)Cl composite membrane and catalytic action in the oxidative dehydrogenation of ethane.

2 Experimental

2.1 Materials and membrane preparation

MgO was prepared by precipitation of magnesium nitrate hexahydrate (Alfa Aesar, 98%) with ammonium oxalate (ACROS Organics, 99.5%). Aqueous $Mg(NO_3)_2$ and ammonium oxalate (1.2 fold excess) was delivered separately via teflon line using peristaltic pump to 50 cm^3 water. The suspension was stirred (600 rpm) at ambient temperature overnight to ensure complete precipitation. The solid obtained was separated by filtration, washed with distilled water and dried at 393 K overnight. The dried sample was calcined in air at 973 K (10 K min^{-1}) for 4 h. (9% mol) Dy_2O_3 on MgO was prepared by impregnation of MgO with aqueous $Dy(NO_3)_3$ (Sigma Aldrich, 99.5%). The slurry was stirred (600 rpm) at ambient temperature overnight. The solid sample was obtained by evaporation at 353 K, dried at 393 K overnight and calcined in air at 973 K (10 K min^{-1}) for 4 h. Alkali chlorides (LiCl and KCl) supported on Dy_2O_3-MgO was prepared by impregnation of Dy_2O_3/MgO with aqueous mixture of LiCl and KCl (LiCl/KCl = 1.5 (mol/mol), Alfa Aesar, 99%). The slurry was stirred (600 rpm) at ambient temperature overnight and heated to 353 K for 4 h. The dried sample was calcined in air at 973 K (10 K min−1) for 4 h. The catalyst precursor was sieved (ATM fine test sieves) to 75–150 μm for the fixed bed reaction. The disk-shape membrane (1.0 mm thickness, 13.0 mm diameter) was prepared by pellet pressing of 0.3 g (Dy_2O_3/MgO)-(Li-K)Cl powder under 4 tons for 2 min. The disk-shape membrane was densified by sintering at 4 K min^{-1} to 973 K in air for 2 h.

2.2 Characterisation

Nitrogen physisorption was performed on the Micromeritics ASAP 2020 system and total specific surface area (SSA) calculated using the standard BET method with cumulative pore volume obtained from BJH desorption. Prior to analysis, samples were vacuumed and outgassed at 573 K for 1 h. X-ray diffractograms (XRD) were recorded on a Bruker D5005 X-

ray diffractometer using Cu Kα radiation. Samples were scanned at 0.02° step−1 over the range $20° \leq 2\theta \leq 80°$ at ambient temperature and the diffractograms identified against the JCPDS-ICDD reference standards. The surface morphology and porosity of the disk-shape membrane was examined by a field emission scanning electron microscopy (SEM, Zeiss SUPRA 55-VP) at an acceleration voltage of 10 kV.

2.3 Thermodynamic analysis

Thermodynamic analysis for the gas-phase dehydrogenation of ethane was conducted using the Gibbs energy minimization method. The total Gibbs free energy function can be described:

$$G = \sum_{i=1}^{k} n_i G_i^0 + RT \sum_{i=1}^{k} n_i \ln \frac{\hat{\phi}_i y_i P}{P^0} \quad (1)$$

where y_i is the mole fraction of species i, and Φ_i is the fugacity coefficient of species i. The calculation procedure is based on the Lagrange's undetermined multiplier method and subject to constrains of material balance. The minimum Gibbs free energy of each gaseous species can be expressed as the following equations.

$$\Delta G_{fi}^0 + RT \ln \frac{y_i P}{P^0} + \sum_k \lambda_k \alpha_{ik} = 0 \quad (2)$$

$$\sum_i y_i \alpha_{ik} = \frac{A_k}{n} \quad (3)$$

$$\sum_i y_i = 1 \quad (4)$$

The species considered for the oxidative dehydrogenation of ethane include C_2H_6, O_2, C_2H_4, H_2 and H_2O. The thermodynamic equilibrium calculations were performed on Outokumpu HSC Chemistry 5.0 software, using the thermochemical database delivered in the software package. Equilibrium model in the software was used to calculate the equilibrium compositions. The initial amount of ethane was set at 1 mol. Thermodynamic analysis condition was 1 atm, 873–973 K and $O_2/C_2H_6 = 0–0.5$.

2.4 Catalytic procedures

Membrane reactions (oxygen permeation and oxidative dehydrogenation of ethane) were carried out at atmospheric pressure (T = 873–1048 K) in a vertical high temperature membrane reactor. The schematic diagram of the membrane reactor is shown in Fig. 1. The disk-shape membrane was sealed between two dense alumina tubes (Precision ceramics, 8 mm i.d.) using gold conductor paste (Heraeus) and heated at 4 K min^{-1} to 973 K or 1073 K for 12 h to ensure gastight leak. The effective permeable area is 0.2–0.4 cm^2. 10 cm^3 min^{-1} (Brooks mass flow controlled) 10–20% v/v O_2/N_2 (BOC, 99.99%) was fed to the oxygen-rich membrane compartment; Ar (2–10 cm^3 min^{-1}, BOC, 99.99%) as a sweep gas, He (1 cm^3 min^{-1}, BOC, 99.99%) as internal standard, ethane or ethylene (1–2 cm^3 min^{-1}, BOC, 99.95%) was fed to the reaction side. The fixed bed reaction was conducted in a continuous flow tubular reactor (8 mm i.d.). Catalysts (0.02 g) were diluted with ground quartz (75–150 μm) to maintain isothermal conditions. Mixtures of ethane or ethylene (2 cm^3 min^{-1}), O_2 (1 cm^3 min^{-1}), Ar (10–20 cm^3 min^{-1}) and He (1 cm^3 min^{-1}) were fed to the reactor. The effluent was analysed using online gas chromatography (Shimadzu 2014) equipped with a 0.5 cm^3 sampling loop, thermal conductive detector (TCD) and flame ionization detector (FID),

employing serial Hayesep Q (3.0 m × 2.1 mm i.d.) and Molecular Sieve 5A packed columns (2.0 m × 2.1 mm i.d.). Data acquisition and manipulation were performed using GC solution Lite (Version 2.4) chromatography data system. Data acquisition and manipulation were performed using GC solution Lite (Version 2.4) chromatography data system. Oxygen permeation influx ($J(O_2)$, μmol s^{-1} cm^{-2}) was defined as reported elsewhere [36] and given below:

$$J_{O_2} = \frac{F_{O_2} - F_{N_2} \times (28/32)^{1/2} \times (1/9)}{A} \tag{5}$$

where $F(O_2)$ and $F(N_2)$ refers to molar flow rate of oxygen and nitrogen measured in the gas on the sweep side; A is effective permeation area (cm^2). Ethane fractional conversion ($X(C_2H_6)$) was defined as reported elsewhere [1] and presented below:

$$X_{C_2H_6}(-) = 1 - \frac{2\left[C_2H_6\right]_{out}}{2\left[C_2H_6\right]_{out} + 2\left[C_2H_4\right]_{out} + \left[CH_4\right]_{out} + \left[CO_2\right]_{out} + \left[CO\right]_{out}} \tag{6}$$

and product j selectivity (S_j) was defined by:

$$S_j(\%) = \frac{\left[product\ j\right]_{out}}{\left[C_2H_6\right]_{in} - \left[C_2H_6\right]_{out}} \times 100 \tag{7}$$

Yield to ethylene ($Y(C_2H_4)$) was calculated using:

$$Y_{C_2H_4}(\%) = X_{C_2H_6} \times S_{C_2H_4} \tag{8}$$

Specific ethylene formation rate (R(C_2H_4), mmol s^{-1} cm^{-2}) was obtained from:

$$R_{C_2H_4} = \frac{[C_2H_6]_{in} \times X_{C_2H_6} \times S_{C_2H_4}}{A} \quad (9)$$

where subscripts “in” and “out” refer to the inlet and outlet gas streams, respectively.

Repeated reactions delivered data reproducibility and carbon balance within 5%.

3 Results and discussion

3.1 Material characterisation

Variation of SSA and pore volume with chlorides content is shown in Fig. 2. Both decrease ($41 \rightarrow 8.2\ m^2\ g^{-1}$, $0.28 \rightarrow 0.022\ cm^3\ g^{-1}$) dramatically with an increase (from 0% to 10.6%) in chlorides content, and tend to be invariable with a further increase of chlorides (10.6% → 23.2%). A calculation based on the pore volume of (Dy_2O_3/MgO) and average density of the chloride salts demonstrates full pore filling of the (Dy_2O_3/MgO) support requires 36.3% chlorides content, larger than the values used in this study. This suggests pores were partially filled and/or blocked during catalyst preparation. A washing of the catalyst to remove chloride can recover 50% of SSA, which confirms part of the pores were filled/blocked as reported elsewhere [29]. In addition, there is evidence showing addition of LiCl resulted in sintering of MgO particles [37], which can also lead to lower SSA and pore volume. XRD patterns of Dy_2O_3/MgO and doped alkali chlorides with different contents are shown in Fig. 3. XRD pattern of Dy_2O_3/MgO is characterised by peaks at $2\theta = 36.9°$, 43.0°, 62.5°, 74.6° and 78.8° due to cubic MgO (1 1 1), (2 0 0), (2 2 0), (3 1 1) and (2 2 2). Additional diffraction signals at $2\theta = 28.9°$, 33.6°, 48.3° and 57.2° correspond to Dy_2O_3 (2 2 2), (4 0 0), (4 4 0) and (6 2 2). XRD analysis of 3.4% chlorides on Dy_2O_3/MgO generated patterns that match those of Dy_2O_3/MgO. There was no detectable peak corresponding to KCl and/or LiCl, which may be due to the crystalline concentration below detection limit. With increasing chlorides content (10.6% → 23.2%), peaks at $2\theta = 28.3°$, 40.4°, 48.3°, 57.2°, 66.4° and 73.6° corresponding to KCl (2 0 0), (2 2 0), (2 2 2), (4 0 0), (4 2 0) and (4 2 2) were observed with stronger signals at higher loadings. But there was still no detectable peak due to LiCl, which can be linked to a loss of Li during calcination at high temperature (973 K) and/or formation of hydrate LiCl at ambient temperature due to strongly hygroscopic properties of LiCl [38]. We can note in-situ XRD analysis of LiKCl/Dy_2O_3-MgO at 100–300 °C revealed diffraction peak at $2\theta = 30°$ due to LiCl, confirming the presence of LiCl, as reported by Gartner et al.

[29]. Surface density and morphology of the disk membrane is critical in determining oxygen diffusion/transport and reactant adsorption/activation, which in turn can impact on the oxidative dehydrogenation [31]. Representative SEM images of the 10.6% LiKCl/Dy_2O_3-MgO sintered disk-shape membrane is shown in Fig. 4. There was no pinhole, crack or Dy_2O_3-MgO crystal grains observed on the membrane surface (Fig. 4(A)). This suggests the disk membrane was highly dense. A number of micro-scale KCl and/or LiCl particles in irregular shape were exposed on the membrane surface (Fig. 4(B)). Gärtner et al. studying oxidative dehydrogenation of ethane over supported chlorides catalysts (T = 898 K), proposed that chlorides were molten generating a molten chlorides-gas phase interface where surface reaction occurred [29].

3.2 Catalysis results

The oxidative dehydrogenation of ethane in membrane reactor requires a membrane that can transport oxygen to the reaction compartment. We first investigate oxygen permeability as a function of temperature using the 10.6% (Li-K)Cl/(Dy_2O_3/MgO) membrane as a representative; the result is shown in Fig. 5. Oxygen permeation influx (0.27–0.31 μmol s^{-1} cm^{-2}) was obtained in the 873–973 K temperature range with an increased influx at higher temperature. At temperature ≥ 625 K, the chlorides were molten generating interfaces between the chlorides and Dy_2O_3/MgO. The bulk chloride phase and the interfacial region can serve as conduction paths for oxygen ions. Higher temperature facilitates oxygen ion conduction, resulting in larger oxygen permeation observed in Fig. 5. We could not find any report on oxygen permeation through (Dy_2O_3/MgO)-(Li-K)Cl composite membrane. But we can note that the oxygen permeation influx obtained in this study was larger than that (0.15 μmol s^{-1} cm^{-2}) reported for Ba-Sr-Ca-Co-Fe-O perovskite membrane under similar conditions (T = 923 K) [39]. Activation energy exacted from Arrhenius plot yielded a value (6 kJ mol^{-1}) that is far lower than that (95–103 kJ mol^{-1}) reported for oxygen permeation through the

$Ba_{0.5}Sr_{0.5}Co_{0.8}Fe_{0.2}O_{3-\delta}$ perovskite membrane [40]. This suggests oxygen permeation through the chlorides membrane is diffusion controlled.

Thermodynamic analysis of the oxidative dehydrogenation of ethane to ethylene as a function of temperature (873–973 K) and O_2/C_2H_6 (0–0.5) was presented in Fig. 6(A). Ethane conversion increased with increasing the reaction temperature (873 → 973 K) in the O_2/C_2H_6 range of 0–0.4. Ethane was completely converted at the stoichiometry $O_2/C_2H_6 = 0.5$ in the investigated temperature range. Ethane conversion was increased at higher O_2/C_2H_6 ratios at each temperature, suggesting the presence of oxygen promoted ethane conversion. The variation of moles of products with O_2/C_2H_6 ratio in the reaction at 923 K as a representative was shown in Fig. 6(B). In the absence of O_2 ($O_2/C_2H_6 = 0$), the amount of C_2H_4 production equaled to that of H_2. There was no H_2O formation, indicating exclusive dehydrogenation of ethane to ethylene ($C_2H_6 \rightarrow C_2H_4 + H_2$). The amount of C_2H_4 and H_2O increased with an increase in the O_2/C_2H_6 ratio; while H_2 was decreased. At $O_2/C_2H_6 = 0.5$, the mole of C_2H_4 equaled to H_2O with no formation of H_2. This suggests oxidative dehydrogenation of ethane ($2\ C_2H_6 + O_2 \rightarrow 2\ C_2H_4 + 2\ H_2O$) was dominant in the reaction network.

Prior to the oxidative dehydrogenation of ethane using the membrane reactor, blank testing was conducted to probe the extent of the homogeneous gas phase reaction. Passage of ethane (in the absence of oxygen) to the empty reactor (T = 923 K) resulted in full selectivity to ethylene at a conversion (0.02, Table 1) that was appreciably lower than the equilibrium values (Fig. 6). Addition of oxygen to the feeding ($C_2H_6/O_2 = 2$) significantly increased ethane conversion (0.02 → 0.59), but lowered ethylene selectivity (to 63.7%) due to generation of carbon dioxide, carbon monoxide and methane. This suggests direct contact of ethane and oxygen promoted ethane combustion to CO_x (CO and CO_2) and cracking to CH_4 in the homogeneous gas phase reaction. Time on-stream conversion and ethylene selectivity with

programmed temperature (873–973 K) for the reaction in the 10.6% (Li-K)Cl/(Dy_2O_3/MgO) membrane reactor is presented in Fig. 7(A). No significant decline in activity was observed at each temperature within 4–6 h. Gärtner et al. [30] reported a rapid loss of ethane conversion (0.6 → 0.3) in the plug flow reaction over MgO supported chlorides (T = 898 K). Our result represents an advancement in terms of stability for the membrane reaction. An increase in temperature (873 → 973 K) resulted in higher conversion. Ethane was converted selectively to ethylene ($S(C_2H_4)$ > 90%) with formation of carbon dioxide as the major carbonaceous by-product, carbon monoxide and methane as the secondary by-products. Significant amount of hydrogen was generated at high temperature (≥923 K). Up to 98% selectivity to ethylene was achieved (at T = 923–948 K), higher than that recorded in the continuous fixed bed reaction under similar conversions (Fig. 7(A)). This represents a significant result for continuous production of ethylene in the light of 80%-93% selectivity reported for the fixed bed reaction over oxide catalysts in the existing literature [1,41]. This value is also higher than that (90–95% selectivity) reported over supported chlorides catalyst in the plug flow reaction [29,30]. The enhanced selectivity can be linked to relatively lower contact time for membrane reactor and separation of oxygen from ethane in the feeding that decreased combustion of ethane to by-products (see Table 1) [31]. Ethylene selectivity increased (91.5% → 98.3%) with increasing temperature (873 → 923 K) with a slight decrease (to 96.9%) at elevated temperature (923 → 973 K). This is in agreement with that observed in the fixed bed reaction over LiCl/MgO [42]. Arrhenius plot using ethylene formation rate (Fig. 7(B)) for reaction over the 10.6% chlorides loaded membrane delivered an apparent activation energy (127 kJ mol^{-1}), close to that (138 kJ mol^{-1}) reported for the plug flow reaction over (Dy_2O_3/MgO) supported chlorides catalyst [29].

Chlorides content can impact on the amount of active species and ethane conversion. Ethylene selectivity and specific formation rate as a function of chlorides content in the temperature

range of 898–948 K is presented in Fig. 8. Dy_2O_3/MgO exhibited lowest selectivity to ethylene, consistent with that reported for the reaction over earth metal oxides [43]. This can be linked to non-selective sites on Dy_2O_3-MgO that promotes formation of alkyl radicals which is facile to be fully oxidised at the oxide surface [44] and/or in the gas phase [43]. Addition of a small amount of chlorides (3.4%) to Dy_2O_3/MgO enhanced ethylene selectivity, indicative of promotional effect of alkali chlorides on selective conversion of ethane to ethylene. This can be attributed to a coverage of non-selective sties by chlorides. In addition, there is evidence showing oxygen ions in the form of hypochlorite (O-Cl) species can react with alkane to selectively produce alkene [41]. A further increase in chlorides content (3.4% → 10.6%) resulted in elevated selectivity with a plateau attained in the chlorides content range of 10.6–23.2%, which can be due to a complete coverage of non-selective sites on Dy_2O_3-MgO surface beyond 10.6% chlorides content. The ethylene formation rate went through a maximum at 10.6% chlorides loading and decreased with increasing chlorides (Fig. 8(B)), suggesting the chloride content is critical in determining the oxidative dehydrogenation of ethane. Kristoffersen et al. [45] studying oxidative dehydrogenation of ethane using ab initio molecule dynamics over LiCl/MgO, proposed oxygen adsorption/dissociation occurred at the LiCl-MgO interface. At lower content of chlorides, Dy_2O_3/MgO particles are not homogeneously covered by the melt chlorides, leading to a lower density for the interface and disconnected migration paths for oxygen ions. At high content, conduction of oxygen ions are suppressed by a thick layer of chlorides due to diffusion constraint, resulting in a smaller amount of oxygen ions available for the reaction with ethane.

To probe the reaction pathway, reaction of ethylene as feedstock was conducted (at 923 K) using the 10.6% (Li-K)Cl/(Dy_2O_3/MgO) membrane. The reaction rate was lower than that recorded in the ethane oxidative dehydrogenation (Table 2), suggesting ethane oxidative dehydrogenation is faster than the ethylene reaction. The reaction generated CO_x (CO and

CO_2) as principal products (selectivity = 90.2%), ethane and methane as secondary products. The ratio of CO_2/CO is similar to that observed in the ethane reaction. This suggests formation of CO_x can proceed via a consecutive ($C_2H_6 \rightarrow C_2H_4 \rightarrow CO_x$) and/or parallel ($CO_x \leftarrow C_2H_6 \rightarrow C_2H_4 \rightarrow CO_x$) mechanism. Argyle et al. [46] studying oxidative dehydrogenation of ethane over vanadium oxide in the fixed bed reactor, reported CO_x was generated from ethane via consecutive conversion of ethylene and direct from ethane in parallel.

Results to this point have established selective production of ethylene from continuous oxidative dehydrogenation of ethane using the (Dy_2O_3/MgO)-(Li-K)Cl composite membrane reactor with highest activity/selectivity achieved over the 10.6% (Li-K)Cl-(Dy_2O_3/MgO) membrane. However, catalytic activity in terms of ethylene yield is still low ($Y(C_2H_4)$ = 33%). We considered the possibility of increasing contact time as a means of enhancing ethylene yield. Ethylene yield was enhanced (to 52%) with lowering Ar flow rate and ethane feeding rate (Table 3). Increasing temperature served to enhance catalytic activity in the oxidative dehydrogenation of ethane as observed in Fig. 5. An increase in temperature (to 1048 K) resulted in higher fractional conversion (to 0.93). However, ethylene selectivity was decreased due to large amounts of CO_2 and CH_4 formation. Ethylene yield was increased (to 64%) with increasing temperature to 1023 K, but decreased (to 62%) at higher temperature (1048 K). Oxygen content in the feed can influence surface reactive species and activity/selectivity [26]. An increase in oxygen feeding concentration in the permeation side increased ethane conversion, but lowered ethylene selectivity and ethylene yield due to enhanced combustion of ethane to carbon dioxide. This is consistent with Zhu's report [3] that higher oxygen content promoted ethane conversion with a loss of ethylene selectivity over Ni-Ta-O catalyst in the continuous fixed bed reaction. To the best of our knowledge, this is the first report of selective ethylene synthesis via oxidative dehydrogenation of ethane using

(Dy_2O_3/MgO)-(Li-K)Cl composite membrane reactor in continuous operation. The highest yield (64%) exceeds that (<55%) reported for the fixed bed reaction over mixed metal oxides ([3,21–28]) and comparable to that (56–74%) for the BSCFO membrane reaction operated at higher temperature (1073–1148 K) [31–33].

4 Conclusion

We demonstrated selective production of ethylene via continuous oxidative dehydrogenation of ethane in an oxygen-transport (Dy_2O_3-MgO) supported alkali chlorides (LiCl and KCl) membrane reactor. Oxygen permeation through the membrane is diffusion controlled, delivering an activation energy of 6 kJ mol^{-1}. Oxygen permeation influx went through a bottom in the 10.6–23.2% chlorides content range. Increased temperature (873 → 973 K) resulted in higher selectivity to ethylene with up to 98% selectivity achieved (at 923–948 K). Ethylene formation rate depends on chlorides amount with a maximum observed at 10.6% chlorides content. Increasing contact time and temperature (to 1023 K) served to further enhance ethylene yield (33% → 64%).

Acknowledgement:

This work was financially supported by European Commission 7th Framework program: BIOGO project (Grant No. 604296). We are grateful to Guannan Hu for the contribution to SEM analysis.

References:

[1] B.Z. Chu, H. An, T.A. Nijhuis, J.C. Schouten and Y. Cheng, A self-redox pure-phase M1 MoVNbTeOx/CeO2 nanocomposite as a highly active catalyst for oxidative dehydrogenation of ethane, J. Catal. 329, 2015, 471–478.

[2] A.M. Avila, Z. Yu, S. Fazli, J.A. Sawada and S.M. Kuznicki, Hydrogen-selective natural mordenite in a membrane reactor for ethane dehydrogenation, Microporous Mesoporous Mater. 190, 2014, 301–308.

[3] H.B. Zhu, D.C. Rosenfeld, D.H. Anjum, S.S. Sangaru, Y. Saih, S. Ould-Chikh and J.M. Basset, Ni-Ta-O mixed oxide catalysts for the low temperature oxidative dehydrogenation of ethane to ethylene, J. Catal. 329, 2015, 291–306.

[4] H.X. Dai, C.F. Ng and C.T. Au, Perovskite-type halo-oxide La1-xSrxFeO3-δXσ (X = F, Cl) catalysts selective for the oxidation of ethane to ethene, J. Catal. 189, 2000, 52–62.

[5] H.X. Dai, C.F. Ng and C.T. Au, YBa2Cu3O7-δXσ (X = F and Cl): highly active and durable catalysts for the selective oxidation of ethane to ethene, J. Catal. 193, 2000, 65–79.

[6] H.X. Dai, C.F. Ng and C.T. Au, Hole-doped La1.85Sr0.15CuO4-δXσ (X = F, Cl) and electron-doped Nd1.85Ce0.15CuO4-δXσ halo-oxide catalysts for the selective oxidation of ethane to ethene, J. Catal. 197, 2001, 251–266.

[7] A. Qiao, V.N. Kalevaru, J. Radnik, A. Duvel, P. Heitjans, A.S.H. Kumar, P.S.S. Prasad, N. Lingaiah and A. Martin, Oxidative dehydrogenation of ethane to ethylene over V2O5/Al2O3 catalysts: effect of source of alumina on the catalytic performance, Ind. Eng. Chem. Res. 53, 2014, 18711–18721.

[8] M.V. Martínez-Huerta, X. Gao, H. Tian, I.E. Wachs, J.L.G. Fierro and M.A. Bañares, Oxidative dehydrogenation of ethane to ethylene over alumina-supported vanadium oxide catalysts: relationship between molecular structures and chemical reactivity, Catal. Today 118, 2006, 279–287.

[9] M.R. Casaletto, L. Lisi, G. Mattogno, P. Patrono, F. Pinzari and G. Ruoppolo, Effect of the preparation technique on the catalytic performances of TiO2 supported vanadium phosphate in the oxidative dehydrogenation of ethane, Catal. Today 91–2, 2004, 271–274.

[10] M.P. Casaletto, L. Lisi, G. Mattogno, P. Patrono and G. Ruoppolo, An XPS study of titania-supported vanadyl phosphate catalysts for the oxidative dehydrogenation of ethane, Appl. Catal. A: Gen 267, 2004, 157–164.

[11] Z.S. Chao and E. Ruckenstein, Noncatalytic and catalytic conversion of ethane over V-Mg oxide catalysts prepared via solid reaction or mesoporous precursors, J. Catal. 222, 2004, 17–31.

[12] G. Tsilomelekis, A. Christodoulakis and S. Boghosian, Support effects on structure and activity of molybdenum oxide catalysts for the oxidative dehydrogenation of ethane, Catal. Today 127, 2007, 139–147.

[13] A. Christodoulakis and S. Boghosian, Molecular structure and activity of molybdena catalysts supported on zirconia for ethane oxidative dehydrogenation studied by operando Raman spectroscopy, J. Catal. 260, 2008, 178–187.

[14] G. Tsilomelekis and S. Boghosian, An operando Raman study of molecular structure and reactivity of molybdenum (VI) oxide supported on anatase for the oxidative dehydrogenation of ethane, PCCP 14, 2012, 2216–2228.

[15] L. Kong, J.M. Li, Z. Zhao, Q.L. Liu, Q.Y. Sun, J. Liu and Y.C. Wei, Oxidative dehydrogenation of ethane to ethylene over Mo-incorporated mesoporous SBA-16 catalysts: the effect of MoOx dispersion, Appl. Catal. A: Gen 510, 2016, 84–97.

[16] X.J. Zhang, J.X. Liu, Y. Jing and Y.C. Xie, Support effects on the catalytic behavior of NiO/Al2O3 for oxidative dehydrogenation of ethane to ethylene, Appl. Catal. A: Gen 240, 2003, 143–150.

[17] K. Nakamura, T. Miyake, T. Konishi and T. Suzuki, Oxidative dehydrogenation of ethane to ethylene over NiO loaded on high surface area MgO, J. Mol. Catal. A: Chem. 260, 2006, 144–151.

[18] B. Solsona, P. Concepción, J.M.L. Nieto, A. Dejoz, J.A. Cecilia, S. Agouram, M.D. Soriano, V. Torres, J. Jiménez-Jiménez and E.R. Castellón, Nickel oxide supported on porous clay heterostructures as selective catalysts for the oxidative dehydrogenation of ethane, Catal. Sci. Technol. 6, 2016, 3419–3429.

[19] E. Asghari, M. Haghighi and F. Rahmani, CO2-oxidative dehydrogenation of ethane to ethylene over Cr/MCM-41 nanocatalyst synthesized via hydrothermal/impregnation methods: influence of chromium content on catalytic properties and performance, J. Mol. Catal. A: Chem. 418, 2016, 115–124.

[20] D.I. Enache, E. Bordes, A. Ensuque and F. Bozon-Verduraz, Vanadium oxide catalysts supported on titania and zirconia: II. Selective oxidation of ethane to acetic acid and ethylene, Appl. Catal. A: Gen 278, 2004, 103–110.

[21] P. Botella, A. Dejoz, J.M.L. Nieto, P. Concepción and M.I. Vázquez, Selective oxidative dehydrogenation of ethane over MoVSbO mixed oxide catalysts, Appl. Catal. A: Gen. 298, 2006, 16–23.

[22] D. Melzer, P.H. Xu, D. Hartmann, Y.Y. Zhu, N.D. Browning, M. Sanchez-Sanchez and J.A. Lercher, Atomic-scale determination of active facets on the MoVTeNb oxide M1 phase and their intrinsic catalytic activity for ethane oxidative dehydrogenation, Angew. Chem. Int. Ed. 55, 2016, 8873–8877.

[23] B.Z. Chu, H. An, X. Chen and Y. Cheng, Phase-pure M1 MoVNbTeOx catalysts with tunable particle size for oxidative dehydrogenation of ethane, Appl. Catal. A: Gen 524, 2016, 56–65.

[24] M.J. Cheng and W.A. Goddard, In silico design of highly selective Mo-V-Te-Nb-O mixed metal oxide catalysts for ammoxidation and oxidative dehydrogenation of propane and ethane, J. Am. Chem. Soc. 137, 2015, 13224–13227.

[25] H.B. Zhu, D.C. Rosenfeld, D.H. Anjum, V. Caps and J.M. Basset, Green synthesis of Ni-Nb oxide catalysts for low-temperature oxidative dehydrogenation of ethane, ChemSusChem 8, 2015, 1254–1263.

[26] H.B. Zhu, D.C. Rosenfeld, M. Harb, D.H. Anjum, M.N. Hedhili, S. Ould-Chikh and J.M. Basset, Ni-M-O (M = Sn, Ti, W) catalysts prepared by a dry mixing method for oxidative dehydrogenation of ethane, ACS Catal. 6, 2016, 2852–2866.

[27] B. Solsona, J.M.L. Nieto, P. Concepción, A. Dejoz, F. Ivars and M.I. Vázquez, Oxidative dehydrogenation of ethane over Ni-W-O mixed metal oxide catalysts, J. Catal. 280, 2011, 28–39.

[28] B. Solsona, P. Concepción, B. Demicol, S. Hernandez, J.J. Delgado, J.J. Calvino and J.M.L. Nieto, Selective oxidative dehydrogenation of ethane over SnO2-promoted NiO catalysts, J. Catal. 295, 2012, 104–114.

[29] C.A. Gärtner, A.C. van Veen and J.A. Lercher, Oxidative dehydrogenation of ethane on dynamically rearranging supported chloride catalysts, J. Am. Chem. Soc. 136, 2014, 12691–12701.

[30] C.A. Gärtner, A.C. van Veen and J.A. Lercher, Highly selective supported alkali chloride catalysts for the oxidative dehydrogenation of ethane, Top. Catal. 57, 2014, 1236–1247.

[31] M.P. Lobera, S. Escolastico and J.M. Serra, High ethylene production through oxidative dehydrogenation of ethane membrane reactors based on fast oxygen-ion conductors, ChemCatChem 3, 2011, 1503–1508.

[32] F.T. Akin and Y.S. Lin, Selective oxidation of ethane to ethylene in a dense tubular membrane reactor, J. Membr. Sci. 209, 2002, 457–467.

[33] H.H. Wang, Y. Cong and W.S. Yang, High selectivity of oxidative dehydrogenation of ethane to ethylene in an oxygen permeable membrane reactor, Chem. Commun. 1468–1469, 2002.

[34] G.Y. Meng, Q.X. Fu, S.W. Zha, C.R. Xia, X.Q. Liu and D.K. Peng, Novel intermediate temperature ceramic fuel cells with doped ceria-based composite electrolytes, Solid State Ionics 148, 2002, 533–537.

[35] C.A. Gärtner, A.C. van Veen and J.A. Lercher, Oxidative dehydrogenation of ethane: common principles and mechanistic aspects, ChemCatChem 5, 2013, 3196–3217.

[36] Z.P. Shao, W.S. Yang, Y. Cong, H. Dong, J.H. Tong and G.X. Xiong, Investigation of the permeation behavior and stability of a Ba0.5Sr0.5Co0.8Fe0.2O3-δ oxygen membrane, J. Membr. Sci. 172, 2000, 177–188.

[37] V.R. Choudhary, S.D. Sansare, A.M. Rajput and D.B. Akolekar, Oxidative conversion of methane to C2 hydrocarbons over Li, Mn, Cd and Zn promoted MgO catalysts: 2. Performance of fresh and reoxidized catalysts in the absence of free oxygen, Appl. Catal. 69, 1991, 187–200.

[38] S. Arndt, G. Laugel, S. Levchenko, R. Horn, M. Baerns, M. Scheffler, R. Schlogl and R. Schomacker, A critical assessment of Li/MgO-based catalysts for the oxidative coupling of methane, Cat. Rev. Sci. Eng. 53, 2011, 424–514.

[39] F. Li, X. Xia, Q.M. Li, Z.H. Liang and S.D. Zhao, The preparation and oxygen permeability of calcium-doped Ba-Sr-Ca-Co-Fe-O perovskite material, Ceram. Int. 41, 2015, 12295–12302.

[40] B.B. He, D. Ding, Y.H. Ling, J.M. Xu and L. Zhao, Efficient modification for enhancing surface activity of Ba0.5Sr0.5Co0.8Fe0.2O3-δ oxygen permeation membrane, J. Membr. Sci. 477, 2015, 7–13.

[41] F. Cavani, N. Ballarini and A. Cericola, Oxidative dehydrogenation of ethane and propane: how far from commercial implementation, Catal. Today 127, 2007, 113–131.

[42] D.J. Wang, M.P. Rosynek and J.H. Lunsford, The effect of chloride ions on a Li+-MgO catalysts for the oxidative dehydrogenation of ethane, J. Catal. 151, 1995, 155–167.

[43] P. Ciambelli, L. Lisi, R. Pirone, G. Ruoppolo and G. Russo, Comparison of behaviour of rare earth containing catalysts in the oxidative dehydrogenation of ethane, Catal. Today 61, 2000, 317–323.

[44] T. Blasco, A. Galli, J.M.L. Nieto and F. Trifiró, Oxidative dehydrogenation of ethane and n-butane on VOx/Al2O3 catalysts, J. Catal. 169, 1997, 203–211.

[45] H.H. Kristoffersen and H. Metiu, Molten LiCl layer supported on MgO: its possible role in enhancing the oxidative dehydrogenation of ethane, J. Phys. Chem. C 119, 2015, 8681–8691.

[46] M.D. Argyle, K.D. Chen, A.T. Bell and E. Iglesia, Ethane oxidative dehydrogenation pathways on vanadium oxide catalysts, J. Phys. Chem. B 106, 2002, 5421–5427.

Table 1: Blank testing of the oxidative dehydrogenation of ethane (T = 923 K, P = 1 atm, Ar = 10 cm^3 min^{-1}, C_2H_6 = 2 cm^3 min^{-1}).

C_2H_6/O_2 (-)	$X_{C_2H_6}$ (-)	$S_{C_2H_4}$ (%)	S_{CO_2} (%)	S_{CH_4} (%)	S_{CO} (%)
2/0	0.02	100	-	-	-
2/1	0.59	63.7	1.6	17.0	17.7

Table 2: Reactant consumption rate and product selectivity for the oxidative dehydrogenation of ethane and the reaction of ethylene over 10.6% (Li-K)Cl-(Dy_2O_3/MgO) membrane (Reaction condition: T = 923 K, P = 1 atm, Ar = 10 cm^3 min^{-1}).

$R_{C_2H_6}$ (mmol s^{-1} cm^{-2})	$S_{C_2H_4}$ (%)	S_{CO_2} (%)	S_{CH_4} (%)	S_{CO} (%)	$R_{C_2H_4}$ (mmol s^{-1} cm^{-2})	$S_{C_2H_6}$ (%)	S_{CO_2} (%)	S_{CH_4} (%)	S_{CO} (%)
0.41	98.3	0.5	0.8	0.4	0.26	0.6	49.3	9.2	40.9

Table 3: Effect of process parameters (temperature, Ar and ethane flow rate) on C_2H_6 conversion, C_2H_4 selectivity and C_2H_4 yield for the oxidative dehydrogenation of ethane over 10.6% (Li-K)Cl-(Dy_2O_3/MgO) membrane.

T (K)	Ar (cm^3 min^{-1})	C_2H_6 (cm^3 min^{-1})	O_2 (%)	$X_{C_2H_6}$ (-)	$S_{C_2H_4}$ (%)	$Y_{C_2H_4}$ (%)
973	10	2	10	0.34	97	33
973	2	2	10	0.48	86	41
973	2	1	10	0.63	82	52
1023	2	1	10	0.85	75	64
1048	2	1	10	0.93	67	62
1023	2	1	20	0.86	72	62

Figure caption

Fig. 1: Schematic diagram of experimental setup.

Fig. 2: Specific surface area (SSA) and pore volume as a function of chlorides content.

Fig. 3: XRD patterns of (I) Dy_2O_3/MgO and Dy_2O_3/MgO supported (II: 3.4%, III: 10.6%, IV: 16.8%, V: 23.2%) chlorides (◆ MgO, ● Dy_2O_3 and ◇ KCl).

Fig. 4: Representative SEM images of the 10.6% (Li-K)Cl-(Dy_2O_3/MgO) membrane.

Fig. 5: Arrhenius plot for oxygen permeation through the 10.6% (Li-K)Cl-(Dy_2O_3/MgO) membrane (T = 873-973 K, P = 1 atm, O_2 = 10%).

Fig. 6: (A) Ethane conversion as a function of reaction temperature (T = 873-973 K, 1 atm) and O_2/C_2H_6 ratio (O_2/C_2H_6 = 0-0.5, P = 1 atm, ■ 0, ● 0.1, ▲ 0.2, ▼ 0.3, ◄ 0.4, ► 0.5) and **(B)** moles of product (■ C_2H_4, ▲ H_2O, ● H_2) as a function of O_2/C_2H_6 ratio (T = 923 K) in the oxidative dehydrogenation of ethane to ethylene.

Fig. 7: (A) Variation of ethane conversion ($X_{C_2H_6}$, square) and selectivity to ethylene ($S_{C_2H_4}$, circle) with time on-stream in the oxidative dehydrogenation of ethane in the 10.6% (Li-K)Cl-(Dy_2O_3/MgO) membrane reactor (solid) and fixed bed reactor (open); **(B)** Arrhenius plot with exacted activation energy (Ea). Reaction conditions: T = 873-973 K, P = 1 atm, O_2 = 10%.

Fig. 8: (A) Ethylene selectivity ($S_{C_2H_4}$) and **(B)** ethylene formation rate ($R_{C_2H_4}$) as a function of chlorides content (●: 898 K, ■: 923 K, ◆: 948 K). Reaction conditions: P = 1 atm, O_2 = 10%.

Fig. 1

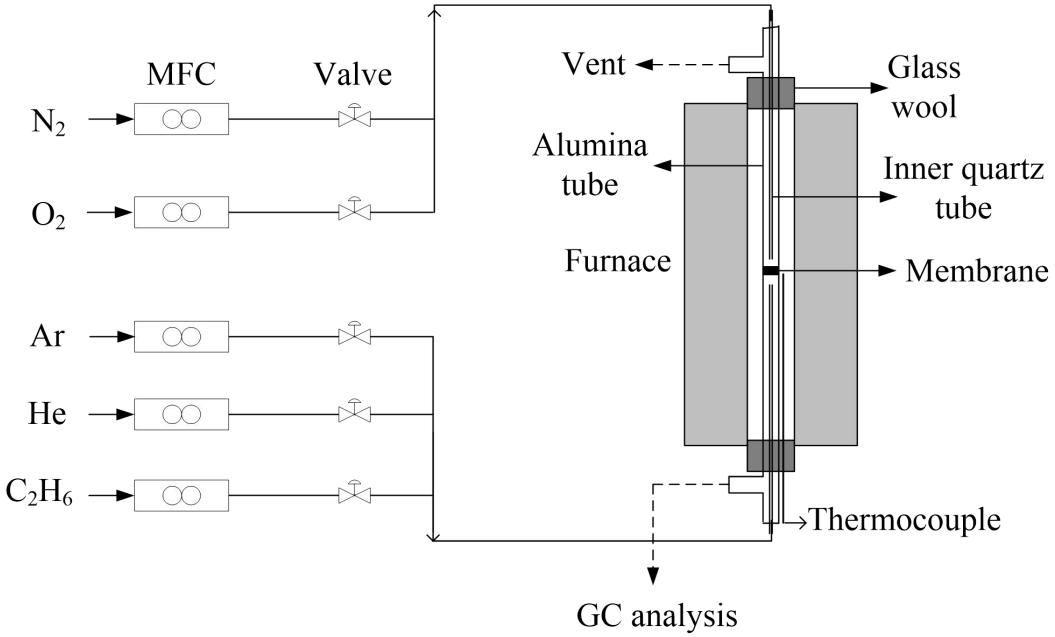
MFC
Valve
N2
O2
Ar
He
C2H6
Vent
Glass wool
Alumina tube
Inner quartz tube
Furnace
Membrane
Thermocouple
GC analysis

Fig. 2

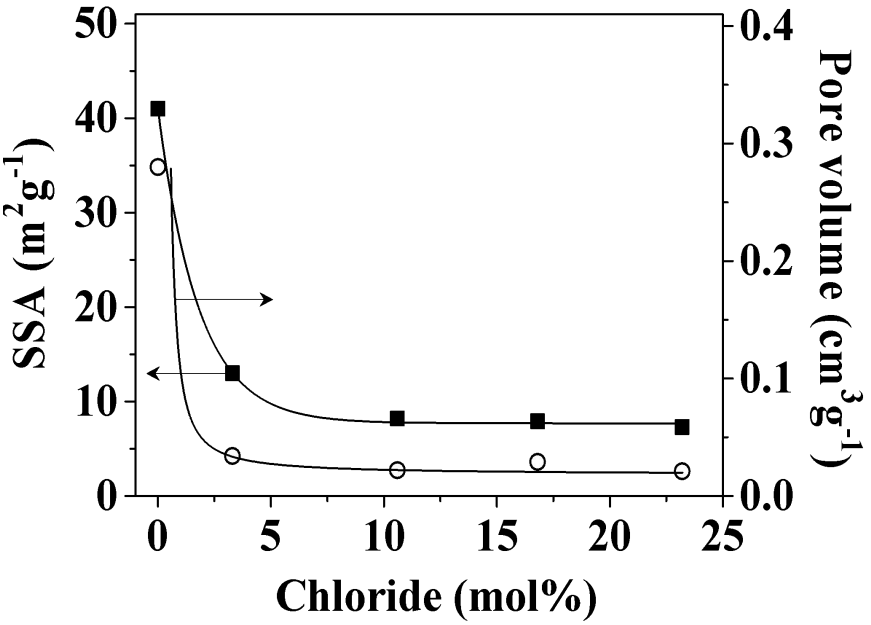
SSA (m^2g^{-1})
Pore volume (cm^3g^{-1})
Chloride (mol%)
0
10
20
30
40
50
0.0
0.1
0.2
0.3
0.4
0
5
10
15
20
25

Fig. 3

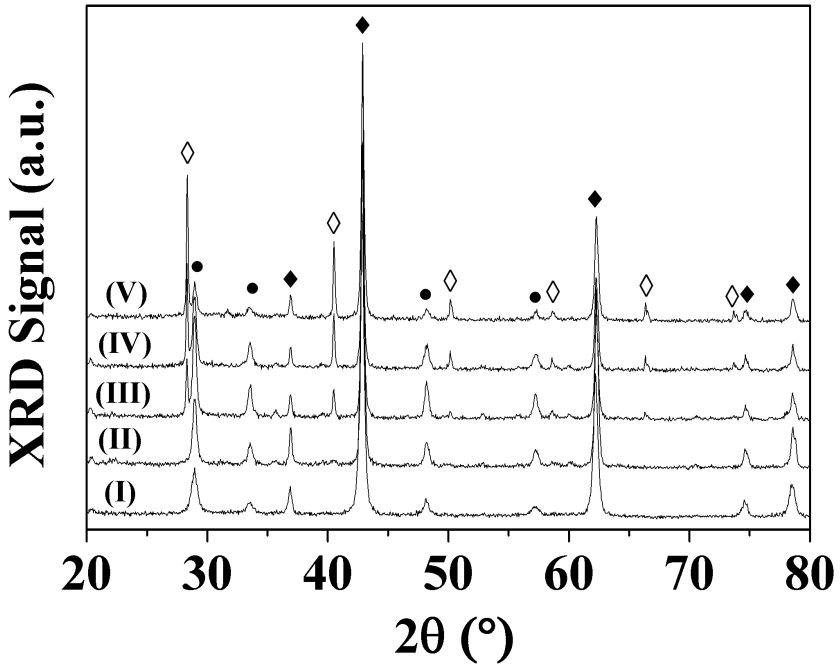

Fig. 4

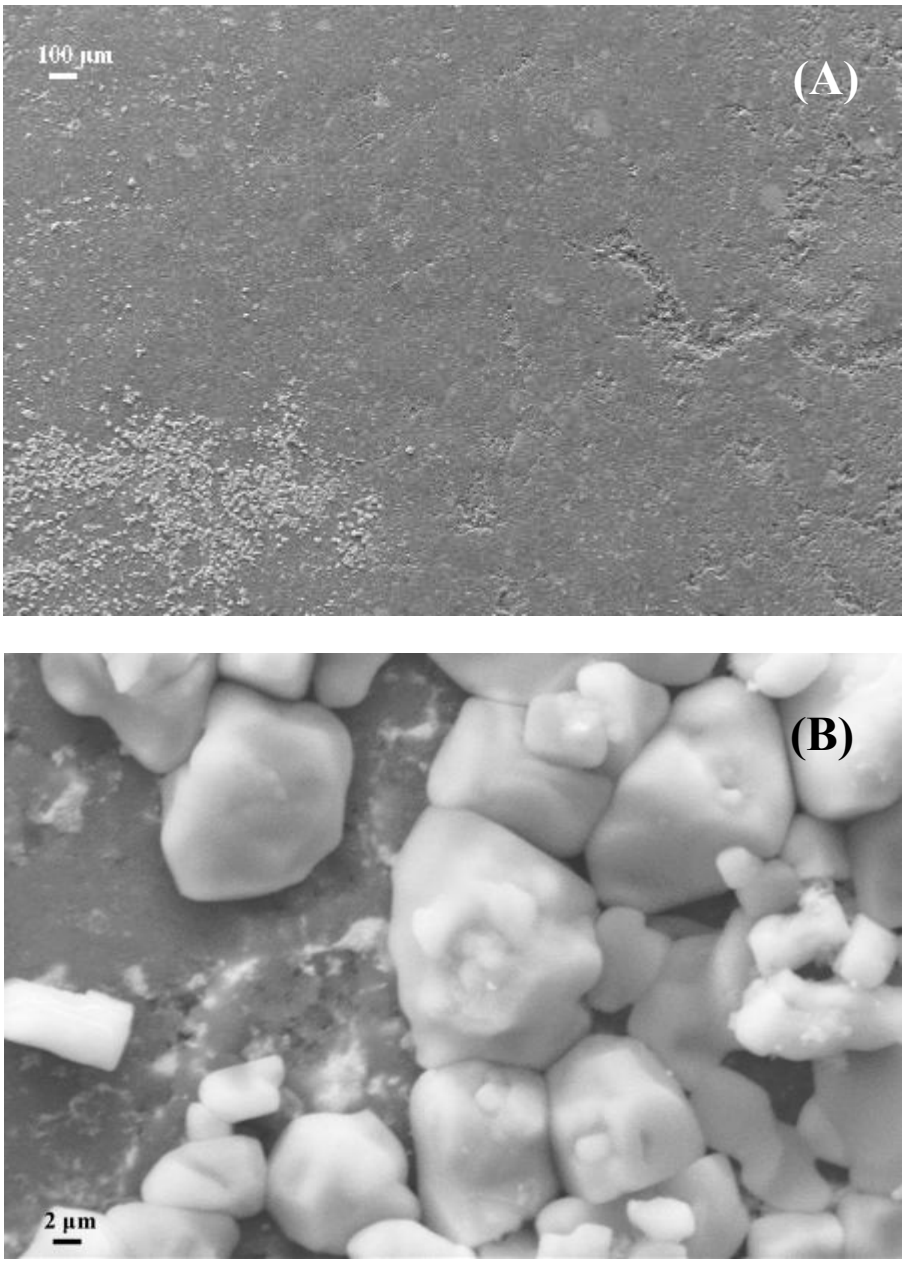

Fig. 5

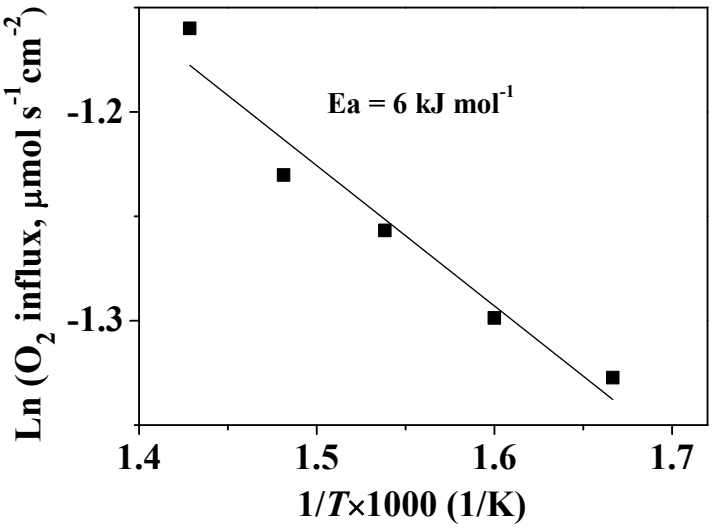

Fig. 6

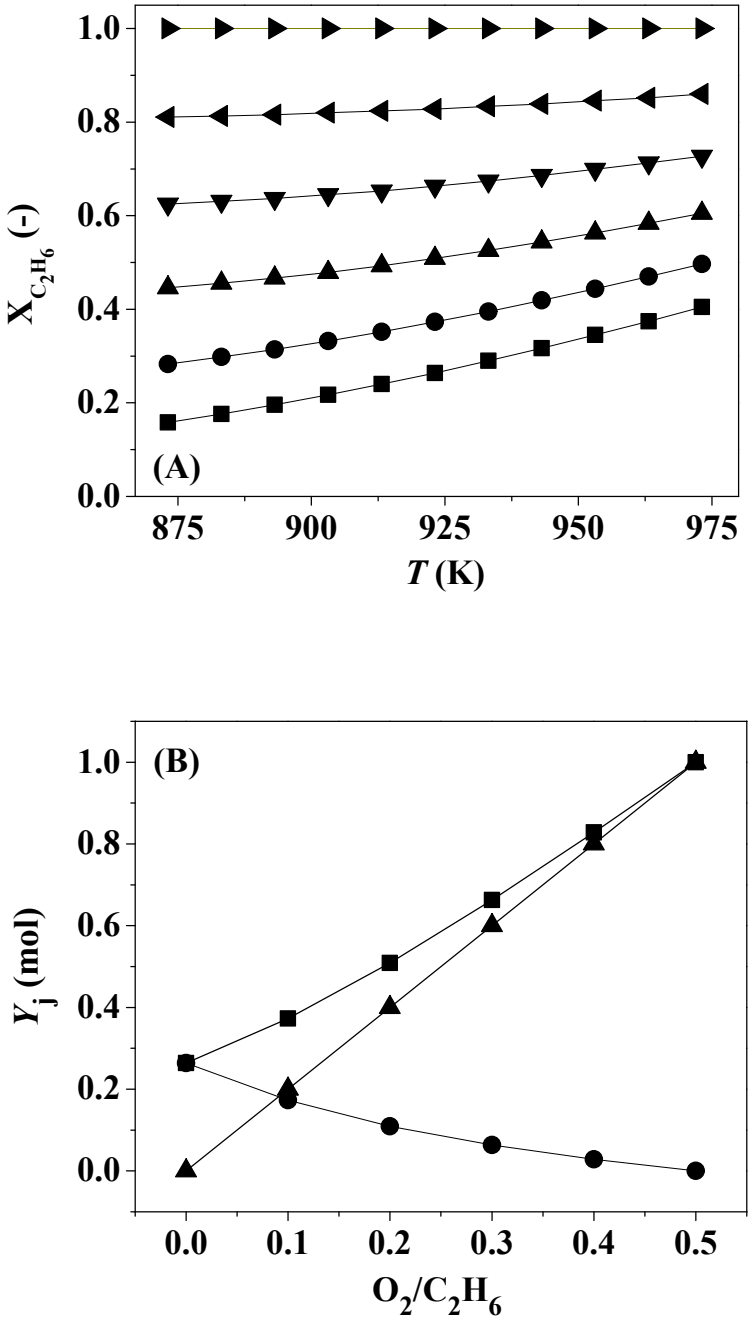
(A)
$X_{C_2H_6}$ (-)
1.0
0.8
0.6
0.4
0.2
0.0
875
900
925
950
975
T (K)
(B)
Y_j (mol)
1.0
0.8
0.6
0.4
0.2
0.0
0.0
0.1
0.2
0.3
0.4
0.5
O_2/C_2H_6

Fig. 7

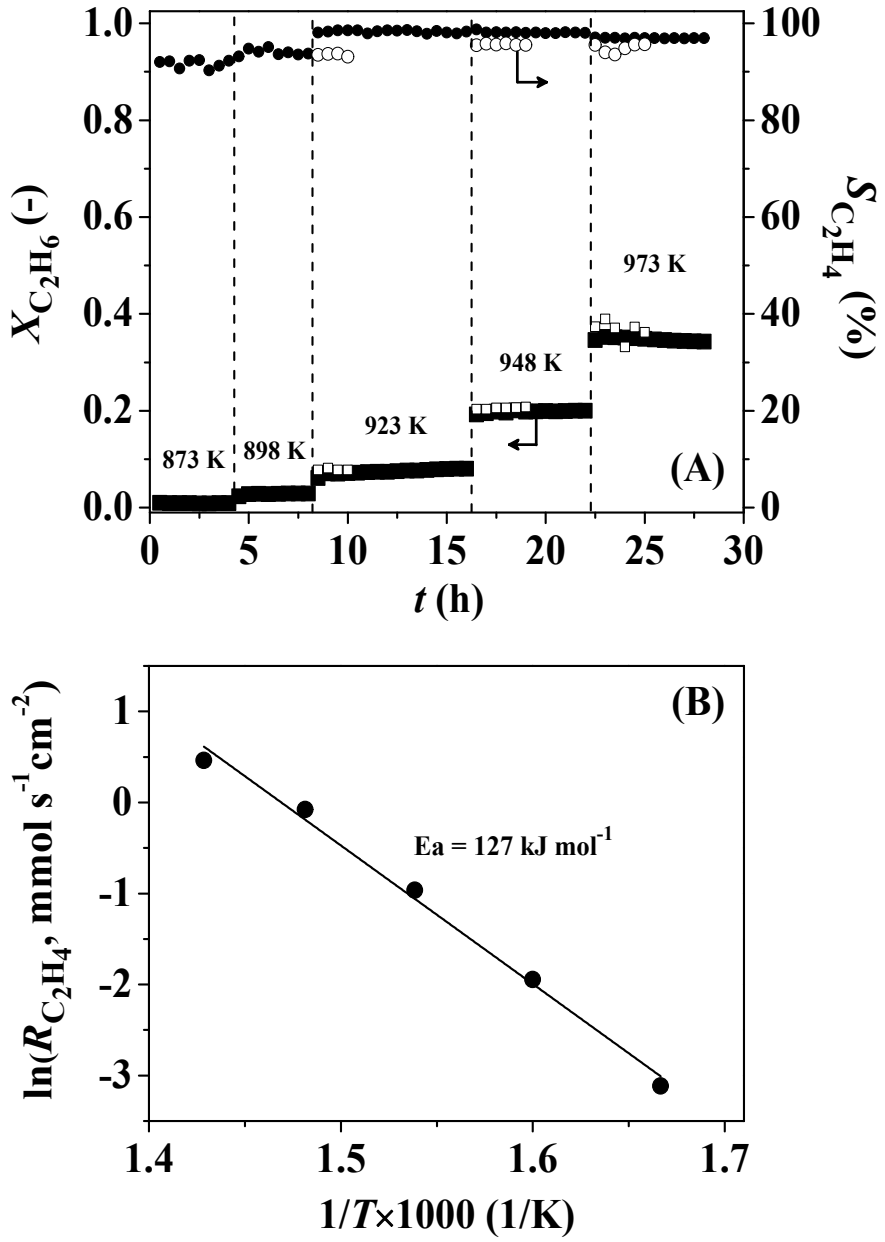
(A)
873 K
898 K
923 K
948 K
973 K
$X_{C_2H_6}$ (-)
$S_{C_2H_4}$ (%)
t (h)
(B)
Ea = 127 kJ mol^{-1}
ln($R_{C_2H_4}$, mmol s^{-1}cm^{-2})
1/T×1000 (1/K)

Fig. 8